ELSEVIER

International Journal of Solids and Structures 41 (2004) 1331–1356

INTERNATIONAL JOURNAL OF SOLIDS and STRUCTURES

www.elsevier.com/locate/ijsolstr

Higher order zig-zag theory for fully coupled thermo-electric–mechanical smart composite plates

Maenghyo Cho *, Jinho Oh

School of Mechanical and Aerospace Engineering, Seoul National University, San 56-1, Shillim-Dong, Kwanak-Gu, Seoul 151-744, South Korea

Received 8 June 2003; received in revised form 20 October 2003

Abstract

A higher order zig-zag plate theory is developed to refine the prediction of the mechanical, thermal, and electric behaviors fully coupled. Both in-plane displacement and temperature fields through the thickness are constructed by superimposing linear zig-zag field to the smooth globally cubic varying field. Smooth parabolic distribution through the thickness is assumed in the out-of-plane displacement field in order to consider transverse normal deformation. Linear zig-zag form is adopted in the electric potential. The layer-dependent degrees of freedom of displacement and temperature fields are expressed in terms of reference primary degrees of freedom by applying interface continuity conditions as well as bounding surface conditions of transverse shear stresses and transverse heat fluxes. Thus the proposed theory is not only accurate but also efficient. Through the numerical examples of coupled and uncoupled analysis, the accuracy and efficiency of the present theory are demonstrated. The present theory is suitable in the predictions of fully coupled behaviors of thick smart composite plate under mechanical, thermal, and electric loads combined.

Keywords: Zig-zag; Smart structure; Thermo; Electric; Mechanical

1. Introduction

Recently, development of integration of piezo-electric materials to composite structures is paid special attentions due to their potential applications to vibration suppression, shape control, noise attenuation and precision positioning. Complexity and full thermo-electric–mechanical coupling of smart composite structures requires efficient and refined models to predict mechanical behaviors under thermal environments.

In the early stage of the development of models, classical/first order shear deformation theory has been employed to predict mechanical behavior of embedded or surface bonded piezo-electric layers (Mindlin, 1968; Tiersten, 1970; Crawley, 1987; Ha et al., 1992; Lee, 1990; Reddy, 1999). However, for the accurate prediction of static and dynamic behavior for general layup configurations of adaptive laminated

* Corresponding author. Fax: +82-2-886-1693/883-1513.
E-mail address: mhcho@snu.ac.kr (M. Cho).

0020-7683/$ - see front matter © 2003 Elsevier Ltd. All rights reserved.
doi:10.1016/j.ijsolstr.2003.10.020

structures, classical and first order shear theory are not adequate. Thus higher order theories with smeared displacements and layerwise electric potential fields (Mitchell and Reddy, 1995; Franco Correia et al., 2000) and full layerwise theories (Saravanos et al., 1997) have been developed. The smeared theory is not enough to describe the deformation behavior through the thickness because it cannot satisfy static continuity conditions at the interfaces between layers. Layerwise theory can adequately describe the deformation behavior through the thickness but it is not computationally efficient because it employs a large number of degrees of freedom which depend upon the number of layers (Reddy and Robbins, 1993, 1994). Carrera (2003) gives a historical review of the zig-zag theories for multilayered plates and shells.

Constitutive equations of most plate theories developed until now are based on the plane stress assumption. They include transverse shear deformation effect but neglect transverse normal deformation effects. It has been well known that the zig-zag pattern of displacement through the thickness under the plane stress assumption provide accurate prediction of deformations and stresses of laminated plates under mechanical loadings (Cho and Parmerter, 1992, 1993; Toledano and Murakami, 1987; Di Sciuva, 1987). However, in thermo-mechanical problem, even in moderate thick plate configurations, the transverse normal deformation effect cannot be neglected since the effect of out-of-plane thermal deformation is equally important compared to those of the in-plane thermal deformations (Ali et al., 1999). In addition, for the complete analysis of adaptive composite laminates under thermal environments, full coupling effects between thermal–mechanical-electricity should be considered for the reliable analysis. Chattopadhyay and co-workers (2000) used a finite element model based on the smeared cubic higher order theory to analyze the smart structures with the full coupling of thermo-mechanical-electricity. However, smeared theories are not adequate in the prediction of deformation behavior and layerwise models and 3-D solid models are computationally too expensive. Thus it is still required to develop accurate and efficient model which can predict the static and dynamic behaviors of smart structures under thermo-electric–mechanical coupled situations.

In the present study, an efficient and accurate higher order zig-zag theory for smart laminated plates is developed. To predict reliable deformation behaviors, transverse normal as well as transverse shear deformations are considered. For the efficient evaluation of the mechanical behaviors, transverse shear stress conditions are pre-imposed in the displacement field to reduce total active degrees of freedom. The temperature field is also obtained by superimposing linear zig-zag field into the global smeared cubic field. The layer-dependent temperature degrees of freedom are suppressed by imposing top and bottom surface thermal conditions as well as interface transverse heat flux continuity conditions. The formulation includes full coupling between thermo-mechanical–electric behaviors. Even though the developed theory is a two-dimensional plate version, full three-dimensional constitutive equations are used for the accurate prediction of the deformation under thermal and electric loads combined.

The developed theory does not have layer-dependent degrees of freedom of displacement field and temperature field but it has layer-dependent degrees of freedom for electric potentials in order to describe arbitrary distributions of electric potential through the thickness of smart structures.

2. Formulation

The Helmholtz free energy may be written as follows and it can be found in the paper of Dokmeci (1980) and more recently Haozhong et al. (2000):

$$F(\varepsilon_{ij}, E_i, \theta) = \tfrac{1}{2}C_{ijkl}\varepsilon_{ij}\varepsilon_{kl} - e_{ijk}E_i\varepsilon_{jk} - \tfrac{1}{2}b_{ij}E_iE_j - k_{ij}\theta\varepsilon_{ij} - d_iE_i\theta - \tfrac{1}{2}a_T\theta^2 \tag{1}$$

In the above equation ε_{ij}, E_i, and θ are the components of the strain tensor, the electric field vector, and the temperature field vector respectively. The coefficients C_{ijkl}, e_{ijk}, and b_{ij} correspond to the elastic constants,

the piezo-electric constants, and the dielectric permittivity. The quantities k_{ij} and d_i are the thermal–mechanical and the thermal–piezo-electric coupling constants respectively. a_T is defined as C_E/T_0. Here, C_E and T_0 are the heat capacity and the initial temperature.

The constitutive equations for fully coupled thermo-mechanical–electric materials are given as,

$$\sigma_{ij} = \frac{\partial F}{\partial \varepsilon_{ij}} = C_{ijkl}\varepsilon_{kl} - e_{ijk}E_k - k_{ij}\theta \tag{2}$$

$$D_i = -\frac{\partial F}{\partial E_i} = e_{ijk}\varepsilon_{jk} + b_{ij}E_j + d_i\theta \tag{3}$$

$$S = -\frac{\partial F}{\partial \theta} = k_{ij}\varepsilon_{ij} + d_iE_i + a_T\theta \tag{4}$$

where σ_{ij} and D_i are the components of the stress tensor and electric displacement vector. S denotes entropy. $\theta = T - T_0$ is the temperature rise from the initial reference temperature T_0. E_i is the components of the electric field vector. b_{ij} is the dielectric permittivity and k_{ij} and d_i refer to the thermal–mechanical and the thermal–piezo-electric coupling constants.

In the case of considering partial coupling, the constitutive equation given in Eq. (2) is only used for the analysis. Based on linear piezo-electricity, E_i can be expressed from a scalar potential function ϕ as follows:

$$E_i = -\phi_{,i} \quad (i = 1, 2, 3) \tag{5}$$

Infinitesimal displacement and strain relationship is used and it is given as,

$$\varepsilon_{ij} = \tfrac{1}{2}(u_{i,j} + u_{j,i}) \tag{6}$$

The configuration of the smart laminated composite plate is shown in Fig. 1.

The governing equations are now derived using the variational principle, assuming no body force, as follows:

$$\delta\pi_u = \delta U_d + \delta U_s + \delta F_1 = -\int_0^{t_0}\int_V (\rho\ddot{u}_i\,\delta u_i + \gamma\dot{u}_i\,\delta u_i + \sigma_{ij}\,\delta\varepsilon_{ij})\,\mathrm{d}V\,\mathrm{d}t + \int_0^{t_0}\int_S t_i\,\delta u_i\,\mathrm{d}S\,\mathrm{d}t = 0 \tag{7}$$

$$\delta\pi_\phi = \delta E + \delta F_2 = -\int_0^{t_0}\int_V D_i\,\delta\phi_{,i}\,\mathrm{d}V\,\mathrm{d}t + \int_0^{t_0}\int_S q_E\,\delta\phi\,\mathrm{d}S\,\mathrm{d}t = 0 \tag{8}$$

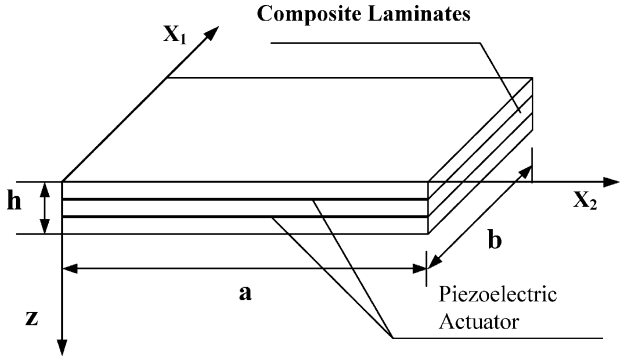

Fig. 1. Configuration of the smart structure laminated composite plates.

$$\delta\pi_\theta = \delta\Theta_k + \delta\Theta_c + \delta F_3 = -\int_0^{t_0}\int_V (\kappa_{ij}\theta_{,i}\,\delta\theta_{,j} + \dot{S}T_0\,\delta\theta)\,\mathrm{d}V\,\mathrm{d}t + \int_0^{t_0}\int_S q_T\,\delta\theta\,\mathrm{d}S\,\mathrm{d}t = 0 \tag{9}$$

where π_u, π_ϕ, and π_θ are energy functionals for the elastic, electrical, and thermal field, respectively. u_i is the displacement vector and $\dot{u}_i$ and $\ddot{u}_i$ are the first and second time derivatives of the displacement vectors. The quantity V is the laminate volume, and the quantity t_0 is the time span for the dynamic deformation. ρ and γ are the density constant and the damping constant of material. The quantities t_i and q_E, q_T are the applied surface traction, the applied charge density, the applied heat flux respectively. κ_{ij} denotes the thermal conductivity. In Eq. (9), S is the entropy and $\dot{S}$ is the derivative of S with respect to time.

For efficient modeling without losing accuracy in the present study, a fully coupled higher-order zig-zag theory is proposed. A zig-zag higher order in-plane displacement field is obtained by superimposing zig-zag linear field to the globally cubic varying field. In order to include the transverse normal effect which is significant in thermo-mechanical problems, the out-of-plane displacement field may be assumed to independently in each layer. However, for the simplicity and efficiency in the present study, the out-of-plane displacement field is assumed as globally parabolic form through the thickness.

The starting displacement field can be written as follows:

$$\begin{aligned} u_\alpha(x_\beta, z, t) &= u_\alpha^o(x_\beta, t) + \psi_\alpha(x_\beta, t)z + \xi_\alpha(x_\beta, t)z^2 + \varphi_\alpha(x_\beta, t)z^3 + \sum_{k=1}^{N-1} S_\alpha^k(x_\beta, t)(z - z_k)H(z - z_k) \\ u_3(x_\alpha, z, t) &= w(x_\alpha, t) + r_1(x_\alpha, t)z + r_2(x_\alpha, t)z^2 \end{aligned} \tag{10}$$

where $H(z - z_k)$ is a Heaviside unit step function. u_α^o and w represent the in-plane displacement and the out-of-plane displacement from the reference plane. ψ_α are the rotation of the normal about x_α axes.

A schematic configuration of the general lamination layup and in-plane displacement field is shown in Fig. 2. By applying top and bottom surface transverse shear free conditions, the following two set of equations are obtained.

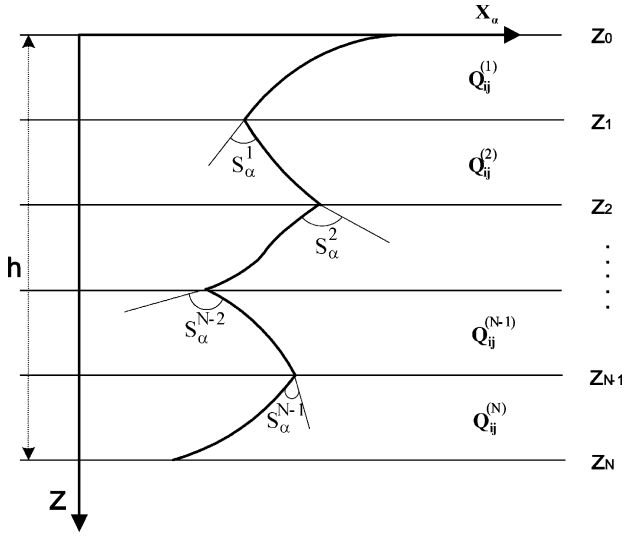

Fig. 2. General lamination layup and in-plane displacement field configurations.

$$\begin{aligned}\gamma_{\alpha 3}|_{z=0} &= \psi_\alpha + w_{,\alpha} = 0 \\ \gamma_{\alpha 3}|_{z=h} &= \psi_\alpha + w_{,\alpha} + 2\xi_\alpha h + 3\varphi_\alpha h^2 + \sum_{k=1}^{N-1} S_\alpha^k + w_{,\alpha} + r_{1,\alpha} h + r_{2,\alpha} h^2 = 0\end{aligned} \tag{11}$$

which, reduces to the following equations.

$$\begin{aligned}\psi_\alpha &= -w_{,\alpha} \\ \xi_\alpha &= -\frac{1}{2h}\left\{3\varphi_\alpha h^2 + \sum_{k=1}^{N-1} S_\alpha^k + r_{1,\alpha} h + r_{2,\alpha} h^2\right\}\end{aligned} \tag{12}$$

Transverse shear strains can be expressed as,

$$\gamma_{\alpha 3} = -\left\{3\varphi_\alpha h + \sum_{k=1}^{N-1} \frac{S_\alpha^k}{h} + r_{1,\alpha} + r_{2,\alpha} h\right\} z + 3\varphi_\alpha z^2 + \sum_{k=1}^{N-1} S_\alpha^k H(z - z_k) + r_{1,\alpha} z + r_{2,\alpha} z^2 \tag{13}$$

Applying transverse shear stress continuity conditions at the interfaces between layers, the change of slope S_α^k can be determined in terms of the primary variables of the reference plane.

$$S_\alpha^k = a_{\alpha\gamma}^k \varphi_\gamma + b_{\alpha\gamma}^k r_{2,\gamma} \tag{14}$$

where S_α^k is the change of slope at each interfaces. The detailed expression for the coefficients $a_{\alpha\gamma}^k$, $b_{\alpha\gamma}^k$ and the derivation of Eq. (14) are given in the Appendix A. To avoid more complexity of the displacement field, the transverse normal stress continuity conditions through the thickness are not imposed in the present modeling.

Substituting of Eqs. (12) and (13) into Eq. (10), the final displacement field reduces to the following form.

$$\begin{aligned}u_\alpha(x_\beta, z, t) &= u_\alpha^o(x_\beta, t) - w_{,\alpha}(x_\beta, t) z - \frac{1}{2h}\left\{3\varphi_\alpha h^2 + \sum_{k=1}^{N-1}(a_{\alpha\gamma}^k \varphi_\gamma + b_{\alpha\gamma}^k r_{2,\gamma}) + r_{1,\alpha}(x_\beta, t) h + r_{2,\alpha}(x_\beta, t) h^2\right\} z^2 \\ &\quad + \varphi_\alpha(x_\beta, t) z^3 + \sum_{k=1}^{N-1}(a_{\alpha\gamma}^k \varphi_\gamma + b_{\alpha\gamma}^k r_{2,\gamma})(z - z_k) H(z - z_k) \\ u_3(x_\alpha, z, t) &= w(x_\alpha, t) + r_1(x_\alpha, t) z + r_2(x_\alpha, t) z^2\end{aligned} \tag{15}$$

The variables in the final displacement field are defined only at the reference plane. The primary variables are u_α^0, w, φ_α, r_1, r_2. Thus the number of the primary variables does not depend upon the number of layers.

Similar to the displacement field construction, the temperature field through the thickness of the plate is obtained by superimposing linear zig-zag field onto the global cubic smooth field. The methodology for imposing transverse shear continuity conditions in Cho and Parmerter (1993) was employed and also transverse heat flux continuity are applied in the similar line of thought. The starting temperature field can be written as follows:

$$\theta(x_\beta, z, t) = \theta_0(x_\beta, t) + \theta_1(x_\beta, t) z + \theta_2(x_\beta, t) z^2 + \theta_3(x_\beta, t) z^3 + \sum_{k=1}^{N-1} \theta^{sk}(x_\beta, t)(z - z_k) H(z - z_k) \tag{16}$$

A schematic of temperature profile is shown in Fig. 3. In general, the plate may be subjected to temperature and heat flux loads at both top and bottom surfaces. Thus the four different sets of thermal boundary conditions on both surfaces are expressed as

$$\text{Set I} \quad \begin{cases} -\kappa_{33}^1 \theta_{,Z} = q_t & \text{at } z = 0 \\ -\kappa_{33}^N \theta_{,Z} = q_b & \text{at } z = h \end{cases} \tag{17a}$$

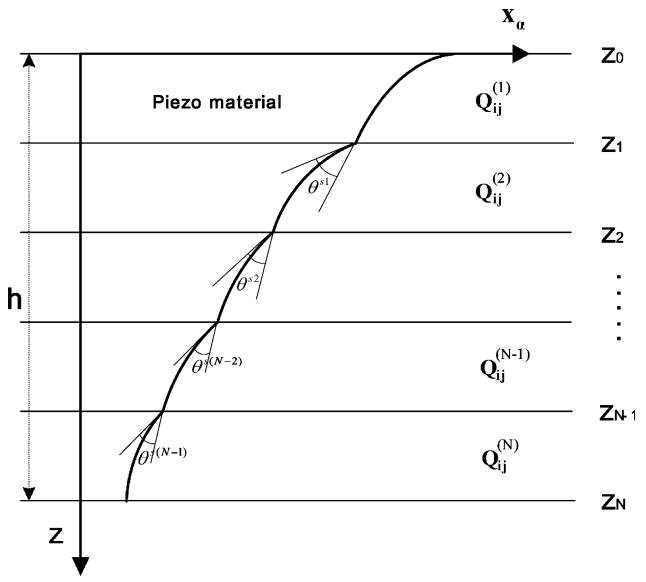

Fig. 3. Temperature field configurations through the thickness.

$$\text{Set II} \quad \begin{cases} -\kappa_{33}^{1}\theta_{,Z} = q_{\mathrm{t}} & \text{at } z = 0 \\ \theta = \overline{T}_{\mathrm{b}} & \text{at } z = h \end{cases} \tag{17b}$$

$$\text{Set III} \quad \begin{cases} \theta = \overline{T}_{\mathrm{t}} & \text{at } z = 0 \\ \theta = \overline{T}_{\mathrm{b}} & \text{at } z = h \end{cases} \tag{17c}$$

$$\text{Set IV} \quad \begin{cases} \theta = \overline{T}_{\mathrm{t}}, & \text{at } z = 0 \\ -\kappa_{33}^{N}\theta_{,z} = q_{\mathrm{b}} & \text{at } z = h \end{cases} \tag{17d}$$

where q_{t} and q_{b} indicate the heat flux applied on top and bottom surfaces, respectively. κ_{33}^{i} denotes the thermal conductivity in the thickness direction in the ith layer. $\overline{T}_{\mathrm{t}}$ and $\overline{T}_{\mathrm{b}}$ are the prescribed temperature values at the top and bottom surfaces. Layer-dependent temperature variable θ^{sk} is determined by the heat flux continuity condition at each interface between layers.

$$\theta^{sk} = C^{k}\theta_3 + B^{k}\theta_2 + d^{k} \tag{18}$$

where C^k and B^k and d^k are functions of heat conduction material properties and thickness of the layers. The detailed expression of Eq. (18) is given in Appendix B. Coefficients f_1, f_2, f_3, f_4 in Appendix B are tracing constants. The tracing constants f_1, f_2, f_3, f_4 are matched to the sets of bounding surface boundary condition as shown in Table 1. For example, Boundary condition set I in Eq. (17a) is given as $f_1 = 1$ and $f_2 = f_3 = f_4 = 0$. Final temperature field is expressed in terms of three primary variables θ_0 and θ_2 and θ_3 in the reference plane and the prescribed heat fluxes and/or prescribed temperatures at top and bottom surfaces.

Substituting thermal boundary condition at the top and bottom surfaces of Eq. (17) into Eq. (16), final four expressions for the temperature field consistent with four different set of boundary conditions given in Eq. (17) can be written as follows:

Table 1
Sets of temperature boundary conditions

	Set I	Set II	Set III	Set IV
f_1	**1**	**0**	**0**	0
f_2	**0**	**1**	**0**	0
f_3	**0**	**0**	**1**	0
f_4	0	0	0	1

$$\theta = \theta_0 - \frac{q_t}{\kappa_{33}^1} z - \frac{1}{2h}\left\{ \frac{q_b}{\kappa_{33}^N} - \frac{q_t}{\kappa_{33}^1} + 3\theta_3 h^2 + \sum_{k=1}^{N-1} \theta^{sk} \right\} z^2 + \theta_3 z^3 + \sum_{k=1}^{N-1} \theta^{sk}(z - z_k) H(z - z_k) \tag{19a}$$

$$\theta = \overline{T}_b + \frac{q_t}{\kappa_{33}^1} h - \theta_2 h^2 - \theta_3 h^3 - \sum_{k=1}^{N-1} \theta^{sk}(h - z^k) - \frac{q_t}{\kappa_{33}^1} z + \theta_2 z^2 + \theta_3 z^3 + \sum_{k=1}^{N-1} \theta^{sk}(z - z_k) H(z - z_k) \tag{19b}$$

$$\theta = \overline{T}_t + \left\{ \frac{\overline{T}_b}{h} - \frac{\overline{T}_t}{h} - \theta_2 h - \theta_3 h^2 - \sum_{k=1}^{N-1} \theta^{sk}(h - z_k)/h \right\} z + \theta_2 z^2 + \theta_3 z^3 + \sum_{k=1}^{N-1} \theta^{sk}(z - z_k) H(z - z_k) \tag{19c}$$

$$\theta = \overline{T}_t + \left\{ -\frac{q_b}{\kappa_{33}^N} - 2\theta_2 h - 3\theta_3 h^2 - \sum_{k=1}^{N-1} \theta^{sk} \right\} z + \theta_2 z^2 + \theta_3 z^3 + \sum_{k=1}^{N-1} \theta^{sk}(z - z_k) H(z - z_k) \tag{19d}$$

The unified temperature field using the tracing constants f_1, f_2, f_3 and f_4 are given as the following single equation (20).

$$\begin{aligned} \theta = {} & f_1\theta_0 + f_2\left\{ \overline{T}_b + \frac{q_t}{\kappa_{33}^1} h - \theta_2 h^2 - \theta_3 h^3 - \sum_{k=1}^{N-1} \theta^{sk}(h - z^k) \right\} + (f_3 + f_4)\overline{T}_t + (f_1 + f_2)\left\{ -\frac{q_t}{\kappa_{33}^1} z \right\} \\ & + f_3\left\{ \frac{\overline{T}_b}{h} - \frac{\overline{T}_t}{h} - \theta_2 h - \theta_3 h^2 - \sum_{k=1}^{N-1} \theta^{sk}(h - z_k)/h \right\} z + f_4\left\{ -\frac{q_b}{\kappa_{33}^N} - 2\theta_2 h - 3\theta_3 h^2 - \sum_{k=1}^{N-1} \theta^{sk} \right\} z \\ & + f_1\left[-\frac{1}{2h}\left\{ \frac{q_b}{\kappa_{33}^N} - \frac{q_t}{\kappa_{33}^1} + 3\theta_3 h^2 + \sum_{k=1}^{N-1} \theta^{sk} \right\} z^2 \right] + (f_2 + f_3 + f_4)\left(\theta_2 z^2\right) + \theta_3 z^3 \\ & + \left\{ \sum_{k=1}^{N-1} \theta^{sk}(z - z_k) H(z - z_k) \right\} \end{aligned} \tag{20}$$

It must be noted that the higher order temperature field defines a non-uniform zig-zag temperature distribution through the thickness of plates. The functions $\theta_0(x, y)$ and $\theta_1(x, y)$ define the in-plane temperature variations. It is important to note that although a linear temperature field can address the in-plane temperature distribution, it cannot satisfy the surface thermal boundary conditions nor the heat flux continuity conditions at the interfaces between layers. Therefore, temperature variations through the thickness, which produce the most important bending deformation, cannot be modeled accurately by the linear temperature field nor smooth cubic field. The present temperature field given in Eq. (19) can describe accurate and simple distribution through the thickness and the pattern is consistent with the cubic zig-zag in-plane displacement field given in Eq. (15). It should be emphasized that if the adjacent layers have severe changes of thermal material properties like sandwich plates or hybrid composite plates, the temperature field given in each equation (19) can predict accurate but significantly different results from those of smeared temperature fields.

The expressions for the electric potential function can be written as follows

$$\phi(x_\beta,z,t)=\sum_{k=1}^{N}\left\{\phi_0^{(k)}(x_\beta,t)+\phi_1^{(k)}(x_\beta,t)(z-z_{k-1})\right\}\{H(z-z_{k-1})-H(z-z_k)\} \tag{21}$$

The description of the electric potential $\phi(x_\beta,z,t)$ is expressed as layer-dependent form using linear zig-zag field through the thickness. Two degrees of freedom are required to express electric potential ϕ in each piezo-electric layer. Since the piezo-electric field exists only in the piezo-electric layers, the formulation of the electric potential is not applicable continuously through the thickness. Even though the layer-dependent potential field is assumed through the thickness, the number of piezo-layers is relatively small compared to the total number of layers. Thus this layer-dependent electric potential field does not increase the number of degrees of freedom significantly. Variational functional based on Eqs. (15) and (19)–(21) can be constructed for general materials with fully coupled constitutive relations given in Eqs. (2)–(4). The equilibrium equations and boundary conditions can be derived from the Hamilton principle. The fully coupled governing equations for the proposed deformation, temperature, and electric field are given here.

Equilibrium equations are derived as,

$$\delta u_\alpha^0: N_{\alpha\beta,\beta\alpha}-I^0\ddot{u}_\alpha-\gamma\dot{u}_\alpha=0 \tag{22a}$$

$$\delta w: M_{\alpha\beta,\beta\alpha}-\rho\ddot{u}_3-\gamma\ddot{u}_3+P=0 \tag{22b}$$

$$\delta\varphi_\alpha: R_{\alpha\beta,\beta}-V_\alpha=0 \tag{22c}$$

$$\delta r_1: N_3-\frac{1}{2}R^{(2)}_{\alpha\beta,\beta\alpha}=\frac{P}{2} \tag{22d}$$

$$\delta r_2: 2M_3+J_{\alpha\beta,\beta\alpha}+I_{\alpha,\alpha}=-\frac{P}{2}h^2 \tag{22e}$$

$$\delta\phi_0^{(k)}: \sum_{k=1}^{N}F^{0(k)}_{\alpha,\alpha}=-q_e^{0(k)} \tag{22f}$$

$$\delta\phi_1^{(k)}: \sum_{k=1}^{N}F^{1(k)}_{\alpha,\alpha}-F_3^{0(k)}=-q_e^{1(k)} \tag{22g}$$

$$\delta\theta_0: N^H_{\alpha\beta,\beta}+V^H_{\beta,\beta}-\dot{T}^H=-(q_\mathrm{t}+q_\mathrm{b}) \tag{22h}$$

$$\begin{aligned}\delta\theta_3: {}&(V_\alpha^{H(1)}+M_3^{H(1)})\left\{-\frac{1}{h}\left(3h^2+\sum_{k=1}^{N-1}C^k\right)\right\}+\left(R^{H(2)}_{\alpha\beta,\beta}+V^{H(2)}_{\beta,\beta}\right)\left\{\frac{1}{2h}\left(3h^2+\sum_{k=1}^{N-1}C^k\right)\right\}\\&+3\left(V_\alpha^{H(2)}+M_3^{H(2)}\right)+\dot{T}^{H(2)}\left\{-\frac{1}{2h}\left(3h^2+\sum_{k=1}^{N-1}C^k\right)\right\}-\left(R^{H(3)}_{\alpha\beta,\beta}+V^{H(3)}_{\beta,\beta}\right)+\dot{T}^{H(3)}\\&-\sum_{k=1}^{N-1}C^k\left(\overline{M}^{Hk}_{\alpha\beta,\beta}+\overline{Q}^{Hk}_{\beta,\beta}\right)+\sum_{k=1}^{N-1}C^k\left(\overline{Q}^{*Hk}_{\alpha}+S^H_3\right)+\sum_{k=1}^{N-1}C^k\dot{E}^{Hk}\\={}&q_\mathrm{b}\left\{-\frac{1}{2h}\left(3h^2+\sum_{k=1}^{N-1}C^k\right)h^2+h^3+\sum_{k=1}^{N-1}C^k(h-z_k)\right\}\end{aligned} \tag{22i}$$

Boundary conditions are given as,

$$N_{\alpha\beta}v_\beta = 0 \text{ or } u_\alpha^0 \quad \text{prescribed} \tag{23a}$$

$$M_{\alpha\beta,\beta}v_\alpha = 0 \text{ or } w \quad \text{prescribed} \tag{23b}$$

$$M_{\alpha\beta}v_\beta = 0 \text{ or } w_{,\alpha} \quad \text{prescribed} \tag{23c}$$

$$R_{\alpha\beta}v_\beta = 0 \text{ or } \varphi_\alpha \quad \text{prescribed} \tag{23d}$$

$$\tfrac{1}{2}R^{(2)}_{\alpha\beta,\beta}v_\alpha = 0 \text{ or } r_1 \quad \text{prescribed} \tag{23e}$$

$$\tfrac{1}{2}R^{(2)}_{\alpha\beta}v_\beta = 0 \text{ or } r_{1,\alpha} \quad \text{prescribed} \tag{23f}$$

$$(I_\alpha + J_{\alpha\beta,\beta})v_\alpha = 0 \text{ or } r_2 \quad \text{prescribed} \tag{23g}$$

$$J_{\alpha\beta}v_\beta = 0 \text{ or } r_{2,\alpha} \quad \text{prescribed} \tag{23h}$$

$$F_\alpha^{0(k)}v_\alpha = 0 \text{ or } \phi_0^{(k)} \quad \text{prescribed} \tag{23i}$$

$$F_\alpha^{1(k)}v_\alpha = 0 \text{ or } \phi_1^{(k)} \quad \text{prescribed} \tag{23j}$$

$$(N^H_{\alpha\beta} + V^H_\beta)v_\beta \text{ or } \theta_0 \quad \text{prescribed} \tag{23k}$$

$$\left(R^{H(2)}_{\alpha\beta} + V^{H(2)}_\beta\right)\left\{-\frac{1}{2h}\left(3h^2 + \sum_{k=1}^{N-1} C^k\right)\right\}v_\beta + \left(R^{H(3)}_{\alpha\beta} + V^{H(3)}_\beta\right)v_\beta + \sum_{k=1}^{N-1}\left(\overline{M}^{Hk}_{\alpha\beta} + \overline{Q}^{Hk}_\beta\right)v_\beta \text{ or } \theta_3 \quad \text{prescribed} \tag{23l}$$

The generalized stress resultants are shown in Eqs. (22) and (23) are given in Appendix C.

The field variables are assumed to have double trigonometric series for simply supported boundary condition as follows.

$$\vec{u} = \begin{Bmatrix} u_1^0 = \sum_{m,n} U \cos\frac{m\pi}{a}x \sin\frac{n\pi}{b}y \\ u_2^0 = \sum_{m,n} V \sin\frac{m\pi}{a}x \cos\frac{n\pi}{b}y \\ w = \sum_{m,n} W \sin\frac{m\pi}{a}x \sin\frac{n\pi}{b}y \\ \varphi_1 = \sum_{m,n} \Omega_1 \cos\frac{m\pi}{a}x \sin\frac{n\pi}{b}y \\ \varphi_2 = \sum_{m,n} \Omega_2 \sin\frac{m\pi}{a}x \cos\frac{n\pi}{b}y \\ r_1 = \sum_{m,n} R_1 \sin\frac{m\pi}{a}x \sin\frac{n\pi}{b}y \\ r_2 = \sum_{m,n} R_2 \sin\frac{m\pi}{a}x \sin\frac{n\pi}{b}y \end{Bmatrix}, \quad \vec{\theta} = \begin{Bmatrix} \theta_0 = \sum_{m,n} \Theta_0 \sin\frac{m\pi}{a}x \sin\frac{n\pi}{b}y \\ \theta_3 = \sum_{m,n} \Theta_3 \sin\frac{m\pi}{a}x \sin\frac{n\pi}{b}y \end{Bmatrix},$$

$$\vec{\phi} = \begin{Bmatrix} \phi_0 = \sum_{m,n} \Phi_0 \sin\frac{m\pi}{a}x \sin\frac{n\pi}{b}y \\ \phi_1 = \sum_{m,n} \Phi_1 \sin\frac{m\pi}{a}x \sin\frac{n\pi}{b}y \end{Bmatrix} \tag{24}$$

$$\vec{F} = \begin{Bmatrix} t_3 = \sum_{m,n} T_3 \sin\frac{m\pi}{a}x \sin\frac{n\pi}{b}y \\ q_e = \sum_{m,n} Q_e \sin\frac{m\pi}{a}x \sin\frac{n\pi}{b}y \\ q_{\mathrm{t}} = \sum_{m,n} Q_{\mathrm{t}} \sin\frac{m\pi}{a}x \sin\frac{n\pi}{b}y \\ q_{\mathrm{b}} = \sum_{m,n} Q_{\mathrm{b}} \sin\frac{m\pi}{a}x \sin\frac{n\pi}{b}y \end{Bmatrix} \tag{25}$$

where t_3 expresses traction in z direction. In order to obtain the solution of equilibrium equation, the above field variables equations (24) and (25) are substituted into Eqs. (7)–(9). Final governing equation for steady state can be written as follows:

$$\begin{bmatrix} K_{uu} & K_{u\phi} & K_{u\theta} \\ K_{\phi u} & K_{\phi\phi} & K_{\phi\theta} \\ K_{\theta u} & K_{\theta\phi} & K_{\theta\theta} \end{bmatrix} \begin{Bmatrix} \vec{u} \\ \vec{\phi} \\ \vec{\theta} \end{Bmatrix} = \left\{ \vec{F} \right\} \tag{26}$$

where $\vec{u}$, $\vec{\phi}$, and $\vec{\theta}$ are the displacement variable vector, the electric potential variable vector, and the temperature variable vector. The detailed expressions of the coefficient K are omitted for the limited space. The field variables are obtained by solving Eq. (26).

3. Numerical examples

Constitutive relations given in Eqs. (2)–(4) account for full coupling between mechanical, thermal and electric fields. Eqs. (5) and (6) are used to replace the strains and the electric fields in Eqs. (2) and (3) by their expressions in terms of the displacements and electric potentials. Eq. (4) may not be used for steady-state problems.

The decoupled theory is obtained by neglecting governing equations given in Eqs. (8) and (9) and neglecting the temperature and electric terms given in Eq. (7). The temperature change and the electric field are treated as external loads in the decoupled theory. The response of the decoupled theory has been studied in our previous work (Cho and Oh, 2002). The previous study (Cho and Oh, 2002) demonstrated that the

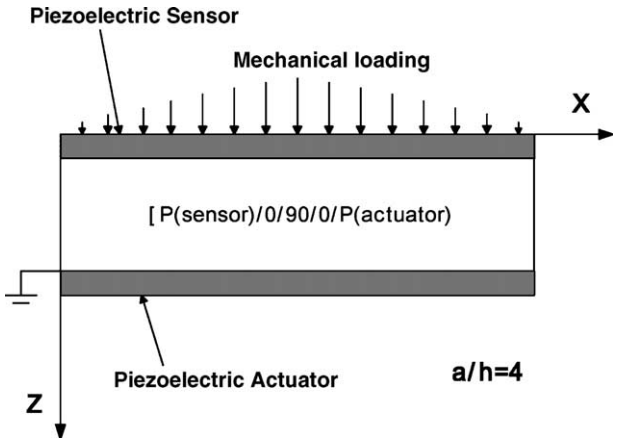

Fig. 4. Plate under mechanical and electric loading.

Table 2
Material properties of the graphite–epoxy and PVDF layer

PVDF layer	Graphite–epoxy layer
$E_1 = E_2 = E_3 = 2 \times 10^9$ (Pa)	$E_1 = 172.37 \times 10^9$ (Pa)
$v = 0.29$	$E_2 = E_3 = 6.895 \times 10^9$(Pa)
$e_{31} = e_{32} = 0.0046$ (C/m^2)	$G_{12} = G_{13} = 3.4475 \times 10^9$ (Pa)
$e_{33} = e_{24} = e_{15} = 0$	$G_{23} = 1.379 \times 10^9$ (Pa)
$b_{11} = b_{22} = b_{33} = 0.1062 \times 10^{-9}$ (F/m)	$v = 0.25$
	$b_{11} = b_{22} = b_{33} = 8.85 \times 10^{-12}$ (F/m)

Table 3
Displacement and stresses for mechanical–electric coupling load comparison between the present and the exact solution (mechanical–electric coupling problem)

S		$\overline{w}$ $(+h/2)$	$\overline{\sigma}_x$ (0)	$\overline{\sigma}_y$ $(+2h/3)$	$\overline{\sigma}_{xy}$ (0)	$\overline{\sigma}_{xz}$ $(+h/2)$	$\overline{\sigma}_{yz}$ $(+h/2)$	$\overline{\sigma}_{zz}$ $(+h/2)$
V = 0 V								
4	Exact (Ray, 1993)	1.99	−0.754	0.532	0.049	0.256	0.217	0.492
	PT	1.94	−0.837	0.583	0.049	0.238	0.229	0.498
10	Exact (Ray, 1993)	0.774	−0.589	0.284	0.0288	0.357	0.123	0.499
	PT	0.751	−0.592	0.291	0.0288	0.356	0.124	0.499
100	Exact (Sheikh, 2001)	0.433	−0.545	0.181	0.021	0.394	0.083	0.5
	PT	0.434	−0.548	0.181	0.021	0.394	0.083	0.5
V = 100 V								
4	Exact (Ray, 1993)	−31.56	11.78	−21.24	−0.728	−3.625	−0.910	−6.68
	PT	−30.6	13.03	−25.10	−1.153	−3.606	−2.163	−8.363
10	Exact (Ray, 1993)	−2.35	1.48	−2.34	−0.058	−0.683	0.336	−0.878
	PT	−2.22	1.49	−2.43	−0.072	−0.686	0.305	−0.932
100	Exact (Sheikh, 2001)	0.411	−0.514	0.158	0.021	0.382	0.086	0.486
	PT	0.412	−0.518	0.158	0.021	0.382	0.086	0.485

The non-dimensional parameters: $(\overline{w}) = w(100E_T)/(q_0 h S^4)$, $(\overline{u}, \overline{v}) = (u, v)(100E_T/q_0 h S^3)$, $(\overline{\sigma}_x, \overline{\sigma}_y, \overline{\sigma}_{xy}) = (\sigma_x, \sigma_y, \sigma_{xy})/q_0 S^2$. $(\overline{\sigma}_{xz}, \overline{\sigma}_{yz}) = (\sigma_{xz}, \sigma_{yz})/q_0 S$, $(\overline{\sigma}_{zz}) = -(\sigma_{zz})/q_0 S$ and $S = a/h$.

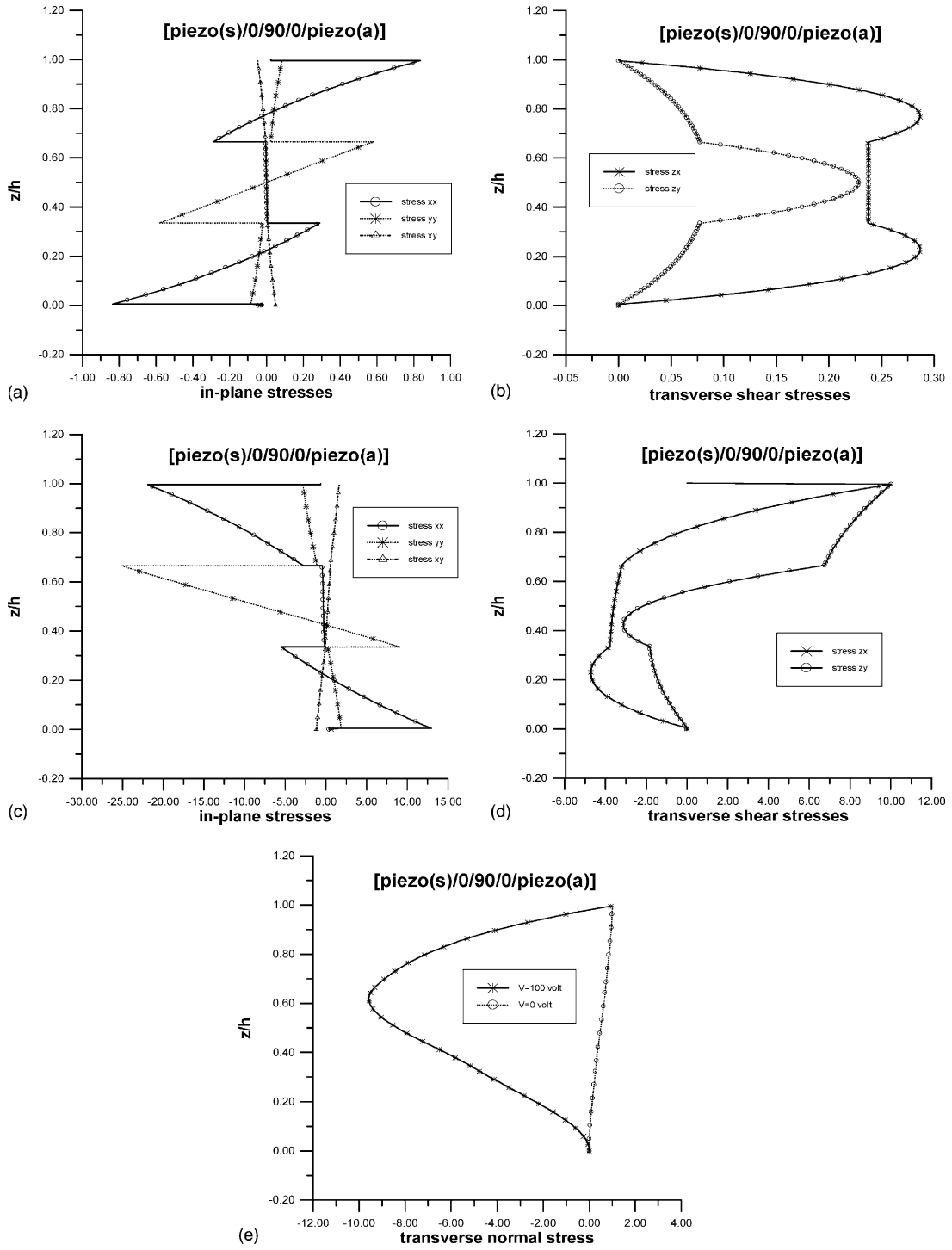

Fig. 5. (a) In-plane stresses ($V = 0$ V), (b) transverse shear stresses ($V = 0$ V), (c) in-plane stresses ($V = 100$ V), (d) transverse shear stresses ($V = 100$ V) and (e) transverse normal stresses.

transverse normal deformation effect can not be neglected under thermal and electric loads. In the present numerical examples, three types of coupled problems are considered. They are mechanical–electric coupled problem, mechanical–electric coupled problem under thermal loads, and fully coupled thermo-electric–mechanical problem. In the numerical example, the coordinates x and y indicates x_1 and x_2, respectively.

3.1. Mechanical–electric coupled/uncoupled problems

Simply supported square plate with [piezo(sensor)/0/90/0/piezo(actuator)] layup is considered. The mechanical loading is doubly sinusoidal and it is applied at the top bounding surface. The schematic of the geometry and loading conditions is shown in Fig. 4. The material properties for this case are given in Table 2. Mechanical load is 1 lb/in.^{2} and it is applied at the top surface of the plate. The voltage $V = 0$ and 100 V are applied at the piezo-actuator located at the bottom of the laminate. Out-of-plane displacements and all the stress components through the thickness for various thickness ratios are given in Table 3. The 3-D elasticity solutions for mechanical–electric coupling problems can be found in Ray et al. (1993) and Sheikh et al. (2001). And it is also given in Table 3 for the comparison. The detailed through-the-thickness stress distributions for thick laminates ($S = 4$) are depicted in Fig. 5. Same non-dimensionalization has been carried out for Table 3 and Fig. 5.

In the thick plate ($S = 4$), out-of-plane displacement has parabolic pattern through the thickness and the prediction of the present higher order zig-zag model correlates very well with the exact elasticity solutions. In moderate thick case ($S = 10$), the deflection is almost uniform through the thickness. Once more, the deflection of the present theory agrees well to the elasticity solution as shown in Table 3.

The in-plane stress distributions through the thickness are shown in Fig. 5(a) and (c). When the voltage $V = 100$ V is applied, the maximum in-plane stresses change their sign.

Transverse stresses are depicted in Fig. 5(b), (d), and (e). Transverse shear and normal stresses are obtained by integrating 3-D local stress equilibrium equations through the thickness of laminates. In the case that the voltage is applied in the actuator layer, the transverse shear stresses of the piezo-sensor layer near the top surface, varies severely to satisfy bounding surface free traction conditions. Applied voltage in the actuator layer in the considered layup configuration amplifies the magnitude of the transverse shear and normal stresses significantly.

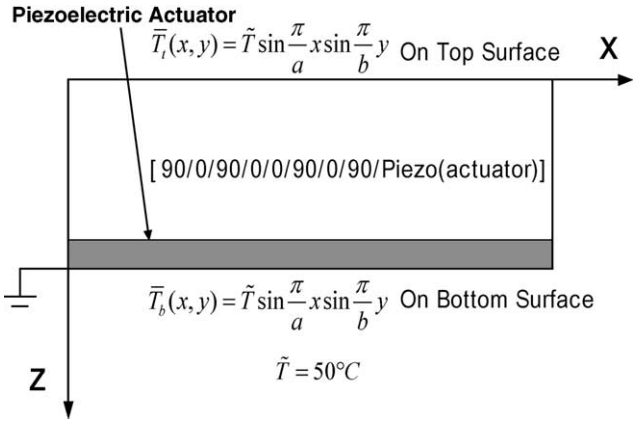

Fig. 6. Plate under electric loading and uniform thermal loading.

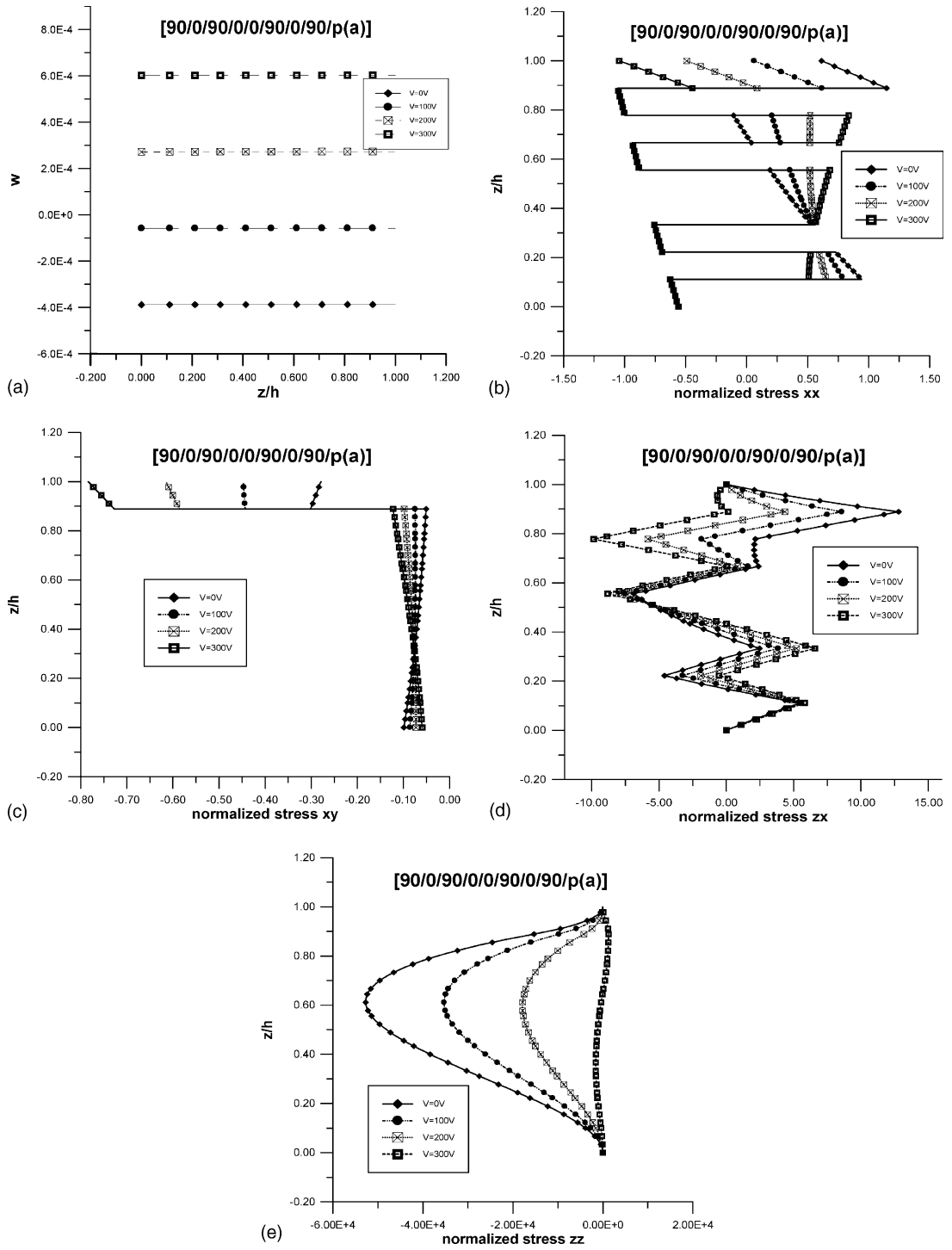

Fig. 7. (a) Out-of-plane displacement, (b) in-plane stress $(\sigma_{xx}/E_{xx})10^4$, (c) in-plane shear stress $(\sigma_{xy}/E_{xx})10^4$, (d) transverse shear stress $(\sigma_{zx}/G_{xy})10^5$ and (e) transverse normal stresses σ_{zz}.

3.2. Mechanical–electric coupling under thermal loads

Two cases are considered in mechanical–electric coupling problem under thermal loads. The first case is for the laminate with piezo-actuator attached on the bottom surface. Fig. 6 shows a schematic of square plate with unsymmetric [90/0/90/0/0/90/0/90/piezo(actuator)] layup. Top and bottom bounding faces are under the uniform temperature rise up to 50 °C. Sinusoidal temperature distributions are considered along the in-plane dimension and they are given in Fig. 6. Boundary conditions are all simple-supported. Fig. 7 shows the deflections and stress distributions under various voltage applied. The out-of-plane displacement is shown in Fig. 7(a). The out-of-plane displacement is almost constant through the thickness of the plate. In the zero voltage applied, the plate is deflected in the upward direction. When small voltage ($V = 100$ V) is applied, the deflection becomes smaller compared to that of the case no voltage is applied. When high voltages ($V = 200$ and 300 V) are applied, the direction of the deflection is changed from upward to downward direction. This observation indicates that the deflection shape can be effectively controlled by the applied high voltage in piezo-actuator layers.

The variation of in-plane normal and shear stresses through the thickness are shown in Fig. 7(b) and (c). As shown in Fig. 7(b), the maximum bending normal stress (σ_{xx}) changes its sign from tension to compression which is consistent with the change of the direction of deflection. The maximum in-plane shear stresses are also significantly changed as the applied electric voltage is getting higher. Transverse shear stress (σ_{zx}) is plotted in Fig. 7(d). As the applied voltage gets higher, the transverse shear stresses change direction. Interlaminar normal stresses change also direction as the applied voltage is getting higher.

The second case is for the laminate with the attached top face piezo-sensor and the attached bottom face piezo-actuator. At the bottom surface, uniform temperature −50 °C is imposed and at the top surface, uniform temperature rise 50 °C is imposed. The layup configuration is [piezo(sensor)/0/90/0/0/90/0/piezo(actuator)] and schematic of the plate is shown in Fig. 8. Since electric voltage $V = 100$ V is applied only at the bottom surface actuator, the normal stress σ_{xx} has the maximum value near the bottom layer. However, the maximum in-plane shear stress appears near the bottom surface even though the magnitude of the shear stress is only 10% of the maximum bending stress as shown in Fig. 9(a) and (b). The transverse shear stress shows zig-zag pattern through the thickness as shown in Fig. 9(c). The transverse normal stress also oscillates significantly through the thickness as shown in Fig. 9(d). Fig. 10 shows the difference between the predictions by the present higher order zig-zag theory and HOT (smeared higher order theory). HOT cannot provide accurate results for thick composite plates. The results of uncoupled zig-zag theory show more accurate stress prediction than HOT does. However, the prediction of the uncoupled cubic zig-zag

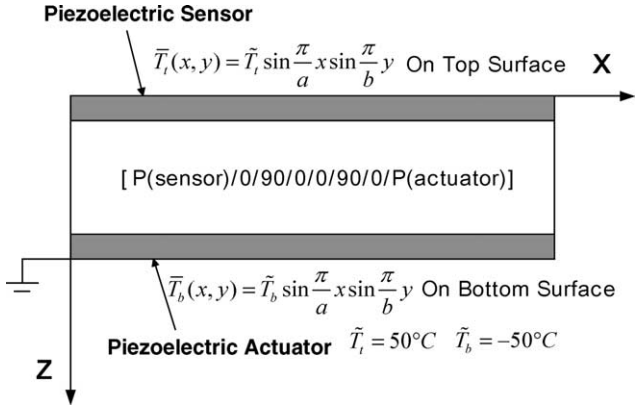

Fig. 8. Plate under electric loading and thermal gradient loading.

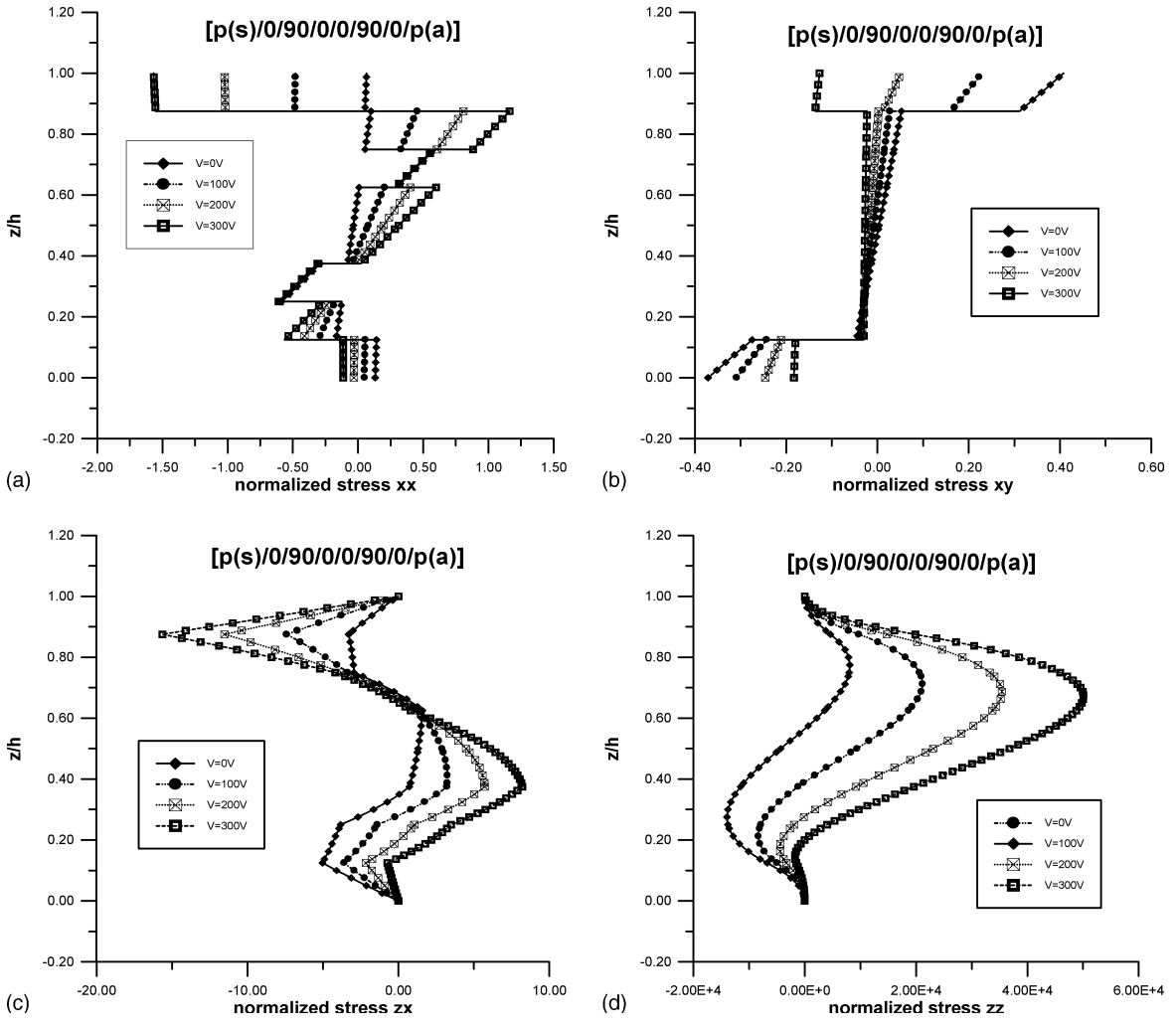

Fig. 9. (a) In-plane stress $(\sigma_{xx}/E_{xx})10^4$, (b) in-plane shear stress $(\sigma_{xy}/E_{xx})10^4$, (c) transverse shear stress $(\sigma_{zx}/G_{xy})10^5$ and (d) transverse normal stresses σ_{zz}.

theory shows discrepancy from that of coupled one because the mechanical energy is transformed into electric and thermal energy in the coupled theory but such energy transformation cannot occur in the uncoupled theory.

3.3. Fully coupled thermo-electric–mechanical problem

For the analysis of fully coupled problems, a problem with the prescribed bounding surface heat flux (set I) of Eq. (17a) is considered. The schematic of the problem is shown in Fig. 11. Heat flux $q_t = 1000$ W/m^2 is applied on the top surface of the plate and bottom surface is adiabatic, i.e. $q_b = 0$ W/m^2. The layup configuration is given as [90/0/90/0/0/90/0/90/piezo(actuator)]. The material properties for this case are given in Table 4. This properties were employed from Haozhong et al. (2000).

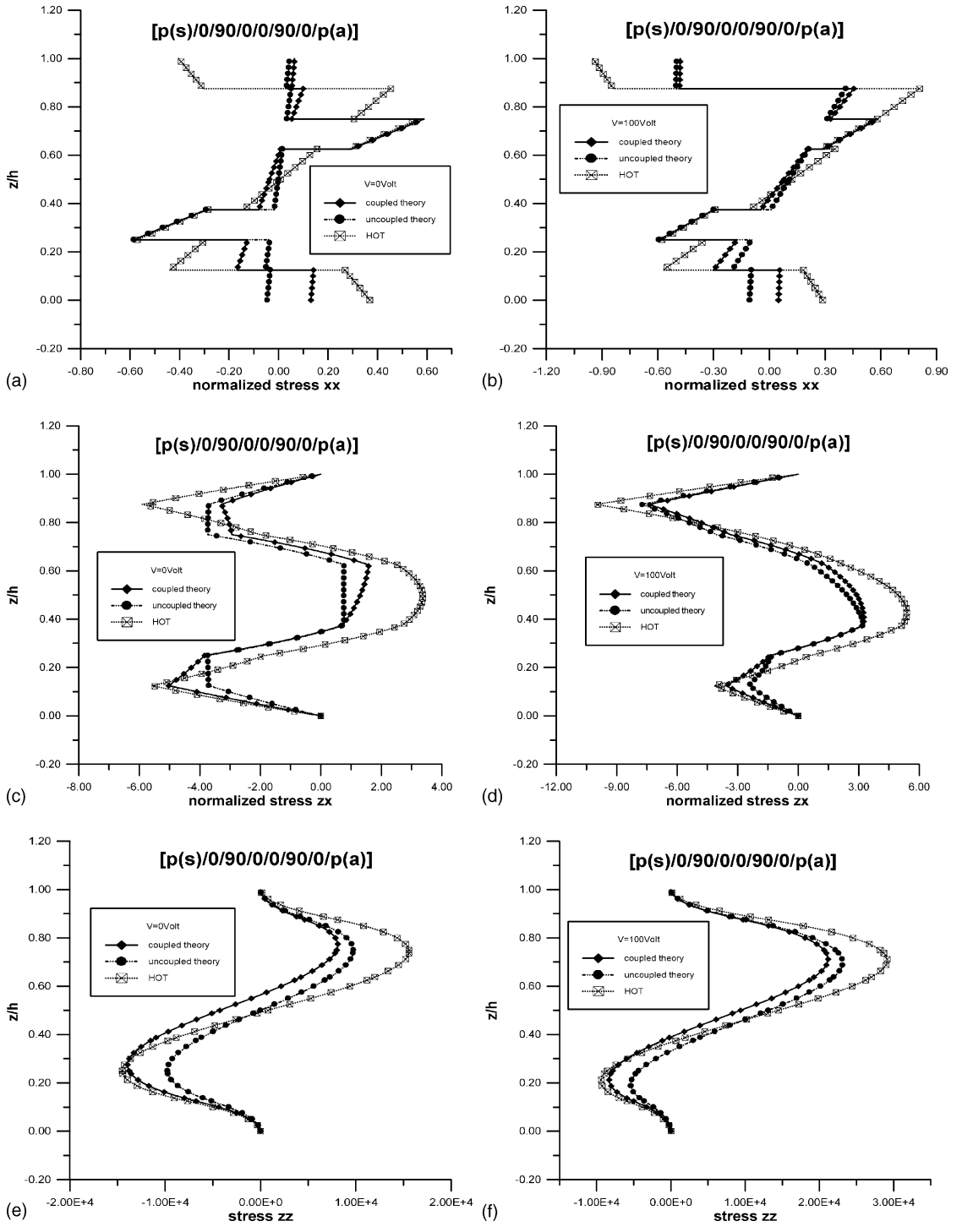

Fig. 10. (a) In-plane stress $(\sigma_{xx}/E_{xx})10^4$, (b) in-plane stress ($V = 100$ V), (c) transverse shear stress $(\sigma_{zx}/G_{xy})10^5$, (d) transverse shear stress ($V = 100$ V), (e) transverse normal stresses σ_{zz} and (f) transverse normal stresses ($V = 100$ V).

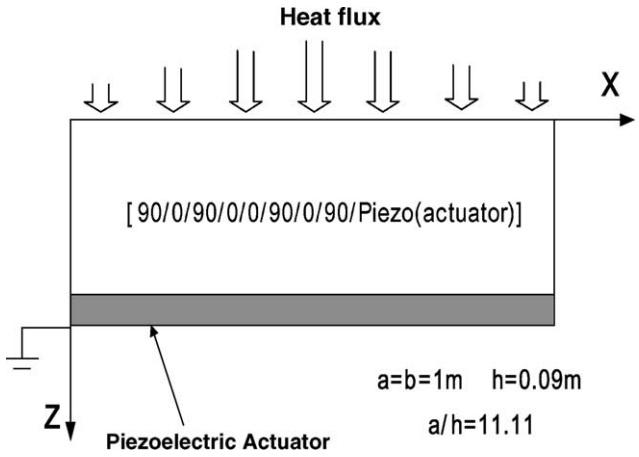

Fig. 11. Plate under electric loading and heat flux loading.

Table 4
Material properties of the graphite–epoxy and PZT layers

PZT layer	Graphite–epoxy layer
$E_1 = E_2 = E_3 = 63 \times 10^9$ (Pa)	$E_1 = 144.23 \times 10^9$ (Pa)
$G_{12} = G_{13} = G_{23} = 24.6 \times 10^9$ (Pa)	$E_2 = E_3 = 9.65 \times 10^9$ (Pa)
$v = 0.28$	$G_{12} = G_{13} = 4.14 \times 10^9$ (Pa)
$\alpha_{11} = \alpha_{22} = \alpha_{33} = 0.9 \times 10^{-6}$ (/°C)	$G_{23} = 3.45 \times 10^9$ (Pa)
$d_{31} = d_{32} = 150 \times 10^{-12}$ (m/V)	$v = 0.3$
$d_{33} = -336.8 \times 10^{-12}$ (m/V)	$\alpha_{11} = 1.1 \times 10^{-6}$ (/°C)
$d_{24} = 0$	$\alpha_{22} = \alpha_{33} = 25.2 \times 10^{-6}$ (/°C)
$d_{15} = 0$	$\kappa_{11} = 4.48$ (W/m °C)
$b_{11} = b_{22} = 15.3 \times 10^{-9}$ (F/m)	$\kappa_{22} = \kappa_{33} = 3.21$ (W/m °C)
$b_{33} = 15.0 \times 10^{-9}$ (F/m)	
$d_3 = 20 \times 10^{-6}$ (C/m^2 °C)	
$\kappa_{11} = \kappa_{22} = \kappa_{33} = 2.1$ (W/m °C)	

The temperature profile through the thickness is obtained by solving coupled heat equation, equilibrium equation and electro-static equation. It shows a smooth distribution through the thickness except the piezo-actuator layer, where the high temperature gradient is observed. If we consider the case with severe thermal property changes through the thickness such as the sandwich or hybrid composite plate, the zig-zag assumed temperature field in the present theory may strongly demonstrate its efficiency and accuracy.

The in-plane normal stresses and transverse shear stress distribution are shown in Fig. 12(b) and (c). Once more, complicated zig-zag patterns are shown in the transverse shear stresses through the thickness. The transverse normal stress distribution is depicted in Fig. 12(d). It shows smooth parabolic shape through the thickness. Fig. 12(e) depicts the out-of-plane displacements through the thickness for fully coupled case and decoupled case. Once more, the parabolic shape of out-of-plane displacements is observed in both cases. Thus the assumption of the present theory on the out-of-plane displacement is appropriate. The results indicate that the coupling effects play an important role in smart composite applications under thermal loads. The deflection predicted by the decoupled theory is always larger, compared to the coupled theory by the amount of 10–20%.

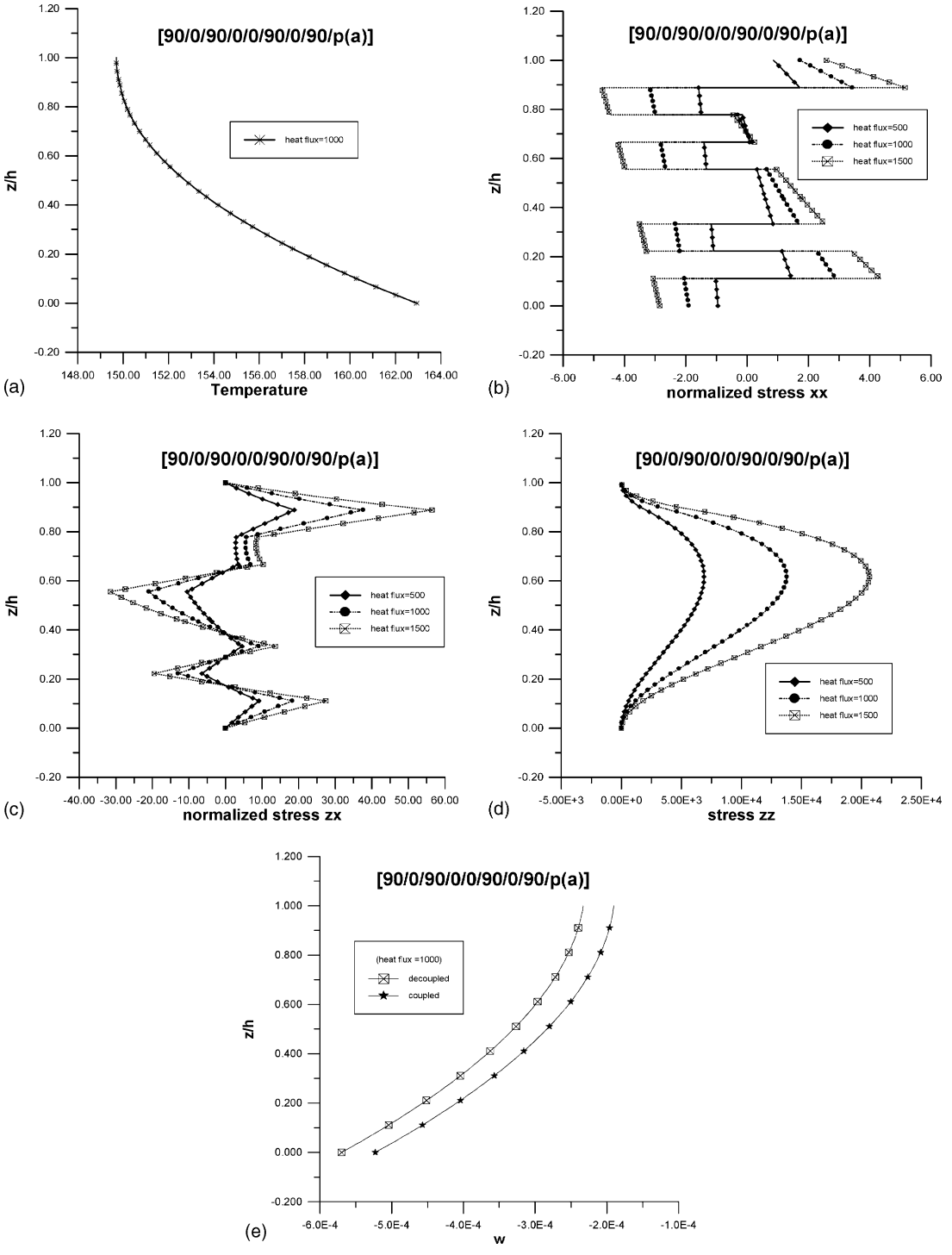

Fig. 12. (a) Temperature field, (b) in-plane stress $(\sigma_{xx}/E_{xx})10^4$, (c) transverse shear stress $(\sigma_{zx}/G_{xy})10^5$, (d) transverse normal stresses σ_{zz} and (e) out-of-plane displacement w.

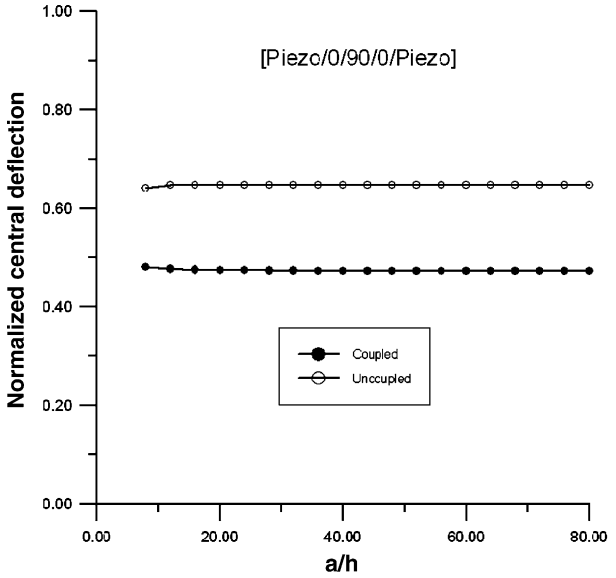

Fig. 13. Deflection top reference surface of coupled and uncoupled theories.

Fig. 13 shows the non-dimensional transverse deflection. vs. the variation of the thickness ratio. The non-dimensional deflections of both the fully coupled theory and decoupled theory decrease as the thickness becomes smaller. The decoupled model overestimates the deflections about 20% compared to those of the coupled one. Thus for the purpose of the reliable analysis and design, full coupling effects between thermo-mechanical–electric behavior need to be considered.

4. Conclusion

A higher order zig-zag theory is developed to enhance the prediction of fully coupled mechanical, thermal, and electric responses of smart composite plates. By imposing transverse shear stress free condition of top and bottom surfaces and interface continuity conditions between layers, the layer-dependent displacement variables can be eliminated. In the similar way, by imposing top and bottom surface heat flux boundary conditions and interface transverse heat flux continuity conditions between layers, the temperature-related variables in each layer are reduced to the temperature degrees of freedom of reference surface. Thus the final form of displacement and temperature fields has only reference primary variables. Layer-dependent degrees of freedom come from the electric potential degrees of freedom only. However, the formulation still keeps the efficiency since the number of the piezo-electric layers is not so large in the practical applications.

Through the numerical examples of uncoupled responses, it is observed that the transverse normal deformation effect is not negligible in the situations that electric and thermal loads are applied. The present theory demonstrated its performance in predicting deformations and interlaminar stresses because it includes the effect of transverse normal deformation. Coupled and uncoupled analyses under thermal loads indicate that uncoupled analysis may overestimate the deflections compared to those of the coupled analysis. The deviation of the results of uncoupled analysis from those of coupled case is up to 20%. Thus full coupling should be considered in the analysis in case of thermal environments.

The present fully coupled theory should be implemented in the finite element framework for the practical thick smart composite plate problem with general geometry, layup, boundary, and loading conditions.

Acknowledgements

This work was supported by Micro Thermal System Research Center of Seoul National University.

Appendix A. Transverse shear stress continuity conditions

The transverse shear continuity conditions for $z > 0$ at $z = z_m$, $m = 1, 2, \ldots, N-1$ ($z_m =$ upper surface of mth layer) are

$$\sigma_{3\alpha}\big|_{z=z_m^-} = \sigma_{3\alpha}\big|_{z=z_m^+}$$

These transverse shear continuity conditions at the interfaces can be expressed by the following matrix equation.

$$\begin{bmatrix} a_{1,1} & a_{1,2} & a_{1,3} & \cdots & \cdots & \cdots & a_{1,2(N-2)} & a_{1,2(N-1)} \\ a_{2,1} & a_{2,2} & a_{2,3} & \cdots & \cdots & \cdots & a_{2,2(N-2)} & a_{2,2(N-1)} \\ a_{3,1} & a_{3,2} & a_{3,3} & \cdots & \cdots & \cdots & a_{3,2(N-2)} & a_{3,2(N-1)} \\ \cdots & \cdots & \cdots & \cdots & \cdots & \cdots & \cdots & \cdots \\ \cdots & \cdots & \cdots & \cdots & \cdots & \cdots & \cdots & \cdots \\ a_{2m-1,1} & a_{2m-1,2} & a_{2m-1,3} & \cdots & \cdots & \cdots & a_{2m-1,2(N-2)} & a_{2m-1,2(N-1)} \\ a_{2m,1} & a_{2m,2} & a_{2m,3} & \cdots & \cdots & \cdots & a_{2m,2(N-2)} & a_{2m,2(N-1)} \\ \cdots & \cdots & \cdots & \cdots & \cdots & \cdots & \cdots & \cdots \\ a_{2(N-2),1} & a_{2(N-2),2} & a_{2(N-2),3} & \cdots & \cdots & \cdots & a_{2(N-2),2(N-2)} & a_{2(N-2),2(N-1)} \end{bmatrix} \begin{Bmatrix} S_1^1 \\ S_1^2 \\ \vdots \\ S_1^{N-1} \\ S_2^1 \\ S_2^2 \\ \vdots \\ S_2^{N-1} \end{Bmatrix}$$

$$= \begin{Bmatrix} \Delta Q_{55}^1(3hz_1 - 3z_1^2) \\ \Delta Q_{45}^1(3hz_1 - 3z_1^2) \\ \vdots \\ \Delta Q_{55}^{m-1}(3hz_{m-1} - 3z_{m-1}^2) \\ \Delta Q_{45}^{m-1}(3hz_{m-1} - 3z_{m-1}^2) \\ \vdots \\ \Delta Q_{55}^{N-1}(3hz_{N-1} - 3z_{N-1}^2) \\ \Delta Q_{45}^{N-1}(3hz_{N-1} - 3z_{N-1}^2) \end{Bmatrix} (\varphi_1) + \begin{Bmatrix} \Delta Q_{45}^1(3hz_1 - 3z_1^2) \\ \Delta Q_{44}^1(3hz_1 - 3z_1^2) \\ \vdots \\ \Delta Q_{45}^{m-1}(3hz_{m-1} - 3z_{m-1}^2) \\ \Delta Q_{44}^{m-1}(3hz_{m-1} - 3z_{m-1}^2) \\ \vdots \\ \Delta Q_{45}^{N-1}(3hz_{N-1} - 3z_{N-1}^2) \\ \Delta Q_{44}^{N-1}(3hz_{N-1} - 3z_{N-1}^2) \end{Bmatrix} (\varphi_2)$$

$$+ \begin{Bmatrix} \Delta Q_{55}^1(hz_1 - z_1^2) \\ \Delta Q_{45}^1(hz_1 - z_1^2) \\ \vdots \\ \Delta Q_{55}^{m-1}(hz_{m-1} - z_{m-1}^2) \\ \Delta Q_{45}^{m-1}(hz_{m-1} - z_{m-1}^2) \\ \vdots \\ \Delta Q_{55}^{N-1}(hz_{N-1} - z_{N-1}^2) \\ \Delta Q_{45}^{N-1}(hz_{N-1} - z_{N-1}^2) \end{Bmatrix} (r_{2,1}) + \begin{Bmatrix} \Delta Q_{45}^1(hz_1 - z_1^2) \\ \Delta Q_{44}^1(hz_1 - z_1^2) \\ \vdots \\ \Delta Q_{45}^{m-1}(hz_{m-1} - z_{m-1}^2) \\ \Delta Q_{44}^{m-1}(hz_{m-1} - z_{m-1}^2) \\ \vdots \\ \Delta Q_{45}^{N-1}(hz_{N-1} - z_{N-1}^2) \\ \Delta Q_{44}^{N-1}(hz_{N-1} - z_{N-1}^2) \end{Bmatrix} (r_{2,2})$$

where $\Delta Q_{ij}^m = Q_{ij}^{m+1} - Q_{ij}^m$.

$(2m-1)$th layer row:

$$a_{2m-1,1}=a_{2m-1,2}=a_{2m-1,3}=\cdots=a_{2m-1,m-1}=\Big(-\frac{z_{m-1}}{h}+1\Big)\Delta Q_{55}^{m-1},\quad a_{2m-1,m}=-\frac{z_{m-1}}{h}\Delta Q_{55}^{m-1}+\Delta Q_{55}^{m}$$

$$a_{2m-1,m+1}=a_{2m-1,m+2}=\cdots=a_{2m-1,N-1}=-\frac{z_{m-1}}{h}\Delta Q_{55}^{m-1}$$

$$a_{2m-1,N}=a_{2m-1,N+1}=a_{2m-1,N+2}=\cdots=a_{2m-1,N+m-2}=\Big(-\frac{z_{m-1}}{h}+1\Big)\Delta Q_{45}^{m-1}$$

$$a_{2m-1,N+m-1}=-\frac{z_{m-1}}{h}\Delta Q_{45}^{m-1}+\Delta Q_{45}^{m}$$

$$a_{2m-1,N+m}=a_{2m-1,N+m+1}=\cdots=a_{2m-1,2(N-1)}=-\frac{z_{m-1}}{h}\Delta Q_{45}^{m-1}$$

$(2m)$th row:

$$a_{2m,1}=a_{2m,2}=a_{2m,3}=\cdots=a_{2m,m-1}=\Big(-\frac{z_{m-1}}{h}+1\Big)\Delta Q_{45}^{m-1},\quad a_{2m,m}=-\frac{z_{m-1}}{h}\Delta Q_{45}^{m-1}+\Delta Q_{45}^{m}$$

$$a_{2m,m+1}=a_{2m,m+2}=\cdots=a_{2m,N-1}=-\frac{z_{m-1}}{h}\Delta Q_{45}^{m-1}$$

$$a_{2m,N}=a_{2m,N+1}=a_{2m,N+2}=\cdots=a_{2m,N+m-2}=\Big(-\frac{z_{m-1}}{h}+1\Big)\Delta Q_{44}^{m-1}$$

$$a_{2m,N+m-1}=-\frac{z_{m-1}}{h}\Delta Q_{44}^{m-1}+\Delta Q_{44}^{m},\quad a_{2m,N+m}=a_{2m,N+m+1}=\cdots=a_{2m,2(N-1)}=-\frac{z_{m-1}}{h}\Delta Q_{44}^{m-1}$$

These equations are of the form

$$[A]\{S\}=[B_1](\varphi_1)+[B_2](\varphi_2)+[C_1](r_{2,1})+[C_2](r_{2,2})$$

where $[A]:2(N-1)\times 2(N-1)[B_1]$, $[B_1]:2(N-1)\times 1[C_1]$, $[C_1]:2(N-1)\times 1$, $[S]:2(N-1)\times 1$, $\{S\}=[A]^{-1}[B_1](\varphi_1)+[A]^{-1}[B_2](\varphi_2)+[A]^{-1}[C_1](r_{2,1})+[A]^{-1}[C_2](r_{2,2})$.

Therefore

$$S_\alpha^k=a_{\alpha\gamma}^k\varphi_\gamma+b_{\alpha\gamma}^k r_{2,\gamma}$$

where, $a_{11}^k=k$th row of $[A]^{-1}[B_1]$, $a_{12}^k=k$th row of $[A]^{-1}[B_2]$, $a_{21}^k=(N-1+k)$th row of $[A]^{-1}[B_1]$, $a_{22}^k=(N-1+k)$th row of $[A]^{-1}[B_2]$, $b_{11}^k=k$th row of $[A]^{-1}[C_1]$, $b_{12}^k=k$th row of $[A]^{-1}[C_2]$ $b_{21}^k=(N-1+k)$th row of $[A]^{-1}[C_1]$, $b_{22}^k=(N-1+k)$th row of $[A]^{-1}[C_2]$.

Appendix B. Heat flux continuity conditions

The heat flux continuity conditions for $z>0$ at $z=z_m$, $m=1,2,\ldots,N-1$ ($z_m=$ upper surface of mth layer) are

$$q_{z=z_m^-}=q_{z=z_m^+}$$

These heat flux continuity conditions at the interfaces can be expressed by the following matrix equation.

$$
\begin{bmatrix}
r_{1,1} & r_{1,2} & r_{1,3} & \cdots & \cdots & \cdots & r_{1,N-2} & r_{1,N-1} \\
r_{2,1} & r_{2,2} & r_{2,3} & \cdots & \cdots & \cdots & r_{2,N-2} & r_{2,N-1} \\
r_{3,1} & r_{3,2} & r_{3,3} & \cdots & \cdots & \cdots & r_{3,N-2} & r_{3,N-1} \\
\cdots & \cdots & \cdots & \cdots & \cdots & \cdots & \cdots & \cdots \\
\cdots & \cdots & \cdots & \cdots & \cdots & \cdots & \cdots & \cdots \\
r_{m-1,1} & r_{m-1,2} & r_{m-1,3} & \cdots & \cdots & \cdots & r_{m-1,N-2} & r_{m-1,N-1} \\
r_{m,1} & r_{m,2} & r_{m,3} & \cdots & \cdots & \cdots & r_{m,N-2} & r_{m,N-1} \\
\cdots & \cdots & \cdots & \cdots & \cdots & \cdots & \cdots & \cdots \\
r_{N-1,1} & r_{N-1,2} & r_{N-1,3} & \cdots & \cdots & \cdots & r_{N-2,N-2} & r_{2(N-2),2(N-1)}
\end{bmatrix}
\begin{Bmatrix}
\theta^{s1} \\ \theta^{s2} \\ \vdots \\ \theta^{s(m-1)} \\ \theta^{sm} \\ \theta^{s(m+1)} \\ \vdots \\ \theta^{s(N-1)}
\end{Bmatrix}
$$

$$
= \begin{Bmatrix}
f_1[\Delta\kappa_{33}^1 3hz_1] + f_2[\Delta\kappa_{33}^1 h^2] + f_4[\Delta\kappa_{33}^1 3h^2] - \Delta\kappa_{33}^1 3z_1^2 \\
f_1[\Delta\kappa_{33}^2 3hz_2] + f_2[\Delta\kappa_{33}^2 h^2] + f_4[\Delta\kappa_{33}^2 3h^2] - \Delta\kappa_{33}^2 3z_2^2 \\
\vdots \\
f_1[\Delta\kappa_{33}^{m-1} 3hz_{m-1}] + f_2[\Delta\kappa_{33}^{m-1} h^2] + f_4[\Delta\kappa_{33}^{m-1} 3h^2] - 3\Delta\kappa_{33}^{m-1} z_{m-1}^2 \\
f_1[\Delta\kappa_{33}^m 3hz_m] + f_2[\Delta\kappa_{33}^m h^2] + f_4[\Delta\kappa_{33}^m 3h^2] - 3\Delta\kappa_{33}^m z_m^2 \\
\vdots \\
f_1[\Delta\kappa_{33}^{N-2} 3hz_{N-2}] + f_2[\Delta\kappa_{33}^{N-2} h^2] + f_4[\Delta\kappa_{33}^{N-2} 3h^2] - 3\Delta\kappa_{33}^{N-2} z_{N-2}^2 \\
f_1[\Delta\kappa_{33}^{N-1} 3hz_{N-1}] + f_2[\Delta\kappa_{33}^{N-1} h^2] + f_4[\Delta\kappa_{33}^{N-1} 3h^2] - 3\Delta\kappa_{33}^{N-1} z_{N-1}^2
\end{Bmatrix} (\theta_3)
$$

$$
+ \begin{Bmatrix}
f_2[\Delta\kappa_{33}^1 (h - 2z_1)] + f_3[-2\Delta\kappa_{33}^1 z_1] + f_4[\Delta\kappa_{33}^1 2(h - z_1)] \\
\vdots \\
f_2[\Delta\kappa_{33}^{m-1} (h - 2z_{m-1})] + f_3[-2\Delta\kappa_{33}^{m-1} z_{m-1}] + f_4[\Delta\kappa_{33}^{m-1} 2(h - z_{m-1})] \\
f_2[\Delta\kappa_{33}^m (h - 2z_m)] + f_3[-2\Delta\kappa_{33}^m z_m] + f_4[\Delta\kappa_{33}^m 2(h - z_m)] \\
\vdots \\
f_2[\Delta\kappa_{33}^{N-1} (h - 2z_{N-1})] + f_3[-2\Delta\kappa_{33}^{N-1} z_{N-1}] + f_4[\Delta\kappa_{33}^{N-1} 2(h - z_{N-1})]
\end{Bmatrix} (\theta_2)
$$

$$
+ \begin{Bmatrix}
f_1\left\{\Delta\kappa_{33}^1\left[\frac{q_t}{\kappa_{33}^1} + \frac{1}{h}\left\{\frac{q_b}{\kappa_{33}^N} - \frac{q_t}{\kappa_{33}^1}\right\} z_1\right]\right\} + f_2\left[\frac{\overline{T}_t}{h} - \frac{\overline{T}_b}{h}\right] + f_3\left[\Delta\kappa_{33}^1 \frac{q_t}{\kappa_{33}^1}\right] + f_4\left[\Delta\kappa_{33}^1 \frac{q_b}{\kappa_{33}^N}\right] \\
\vdots \\
f_1\left\{\Delta\kappa_{33}^{m-1}\left[\frac{q_t}{\kappa_{33}^1} + \frac{1}{h}\left\{\frac{q_b}{\kappa_{33}^N} - \frac{q_t}{\kappa_{33}^1}\right\} z_{m-1}\right]\right\} + f_2\left\{\Delta\kappa_{33}^{m-1}\left[\frac{\overline{T}_t}{h} - \frac{\overline{T}_b}{h}\right]\right\} + f_3\left[\Delta\kappa_{33}^{m-1} \frac{q_t}{\kappa_{33}^1}\right] + f_4\left[\Delta\kappa_{33}^{m-1} \frac{q_b}{\kappa_{33}^N}\right] \\
f_1\left\{\Delta\kappa_{33}^m\left[\frac{q_t}{\kappa_{33}^1} + \frac{1}{h}\left\{\frac{q_b}{\kappa_{33}^N} - \frac{q_t}{\kappa_{33}^1}\right\} z_m\right]\right\} + f_2\left\{\Delta\kappa_{33}^m\left[\frac{\overline{T}_t}{h} - \frac{\overline{T}_b}{h}\right]\right\} + f_3\left[\Delta\kappa_{33}^m \frac{q_t}{\kappa_{33}^1}\right] + f_4\left[\Delta\kappa_{33}^m \frac{q_b}{\kappa_{33}^N}\right] \\
\vdots \\
f_1\left\{\Delta\kappa_{33}^{N-1}\left[\frac{q_t}{\kappa_{33}^1} + \frac{1}{h}\left\{\frac{q_b}{\kappa_{33}^N} - \frac{q_t}{\kappa_{33}^1}\right\} z_{N-1}\right]\right\} + f_2\left\{\Delta\kappa_{33}^{N-1}\left[\frac{\overline{T}_t}{h} - \frac{\overline{T}_b}{h}\right]\right\} + f_3\left[\Delta\kappa_{33}^{N-1} \frac{q_t}{\kappa_{33}^1}\right] + f_4\left[\Delta\kappa_{33}^{N-1} \frac{q_b}{\kappa_{33}^N}\right]
\end{Bmatrix}
$$

where $\Delta\kappa_{33}^m = \kappa_{33}^{m+1} - \kappa_{33}^m$.

$(m-1)$th layer row: $i = 1, 2, \ldots, m-2$

$$
r_{m-1,i} = f_1\left(-\frac{z_{m-1}}{h}\right)\Delta\kappa_{33}^{m-1} + f_2\left(\Delta\kappa_{33}^{m-1}(z_i - h)\frac{1}{h}\right) + f_4(-\Delta\kappa_{33}^{m-1}) + \Delta\kappa_{33}^{m-1}
$$

$$
r_{m-1,m-1} = f_1\left(-\frac{z_{m-1}}{h}\Delta\kappa_{33}^{m-1}\right) + f_2\left(\Delta\kappa_{33}^{m-1}(z_{m-1} - h)\frac{1}{h}\right) + f_4(-\Delta\kappa_{33}^{m-1}) + \kappa_{33}^m
$$

$j = m, m+1, \ldots, N-1$

$$
r_{m-1,j} = f_1\left(-\frac{z_{m-1}}{h}\Delta\kappa_{33}^{m-1}\right) + f_2\left(\Delta\kappa_{33}^{m-1}(z_j - h)\frac{1}{h}\right) + f_4(-\Delta\kappa_{33}^{m-1})
$$

(m)th row: $i = 1, 2, \ldots, m-1$

$$r_{m,1} = r_{m,2} = r_{m,3} = \cdots = r_{m,m-1} = f_1\Big(-\frac{z_m}{h}\Big)\Delta\kappa_{33}^m + f_2\bigg(\Delta\kappa_{33}^m(z_i - h)\frac{1}{h}\bigg) + f_4(-\Delta\kappa_{33}^m) + \Delta\kappa_{33}^m$$

$$r_{m,m} = f_1\Big(-\frac{z_m}{h}\Delta\kappa_{33}^m\Big) + f_2\bigg(\Delta\kappa_{33}^m(z_m - h)\frac{1}{h}\bigg) + f_4(-\Delta\kappa_{33}^m) + \kappa_{33}^{m+1}$$

$j = m+1, \ldots, N-1$

$$r_{m,m+1} = r_{m,m+2} = \cdots = r_{m,N-1} = f_1\Big(-\frac{z_m}{h}\Delta\kappa_{33}^m\Big) + f_2\bigg(\Delta\kappa_{33}^m(z_j - h)\frac{1}{h}\bigg) + f_4(-\Delta\kappa_{33}^m)$$

These equations are of the form

$$[A]\{\theta^s\} = [C](\theta_3) + [B](\theta_2) + [D]$$

where $[A] : (N-1)\times(N-1)$, $[B] : (N-1)\times 1$, $[C] : (N-1)\times 1$, $[D] : (N-1)\times 1$, $[\theta^s] : (N-1)\times 1$

$$\{\theta^s\} = [A]^{-1}[C](\theta_3) + [A]^{-1}[B](\theta_2) + [A]^{-1}[D]$$

Therefore

$$\theta^{sk} = C^k\theta_3 + B^k\theta_2 + d^k$$

where $C^k = k$th row of $[A]^{-1}[C]$, $B^k = k$th row of $[A]^{-1}[B]$, $d^k = k$th row of $[A]^{-1}[D]$.

Appendix C. Definitions of the resultants

C.1. Resultants

Resultants given in the equilibrium equation (21) and boundary condition (22) are defined as follows.

$$\Big[N_{\alpha\beta} \quad M_{\alpha\beta} \quad R_{\alpha\beta}^{(2)} \quad R_{\alpha\beta}^{(3)}\Big] = \int_0^h \sigma_{\alpha\beta}\big[1 \quad z \quad z^2 \quad z^3\big]\,\mathrm{d}z, \quad \Big[\overline{N}_{\alpha\beta}^i \quad \overline{M}_{\alpha\beta}^i\Big] = \int_0^h \sigma_{\alpha\beta}[1(z-z_i)]H(z-z_i)\,\mathrm{d}z$$

$$\big[V_\alpha^{(1)} \quad V_\alpha^{(2)} \quad Q_\alpha^i\big] = \int_0^h \sigma_{3\alpha}\big[z \quad z^2 \quad H(z-z_i)\big]\,\mathrm{d}z, \quad N_3 = \int_0^h \sigma_{33}\,\mathrm{d}z, \quad M_3 = \int_0^h \sigma_{33}z\,\mathrm{d}z$$

$$J_{\alpha\beta} = -\frac{h}{2}R_{\alpha\beta}^{(2)} + \sum_{k=1}^{N-1} b_{\gamma\alpha}^k\bigg\{\overline{M}_{\gamma\beta}^k - \frac{1}{2h}R_{\gamma\beta}^{(2)}\bigg\}, \quad I_\alpha = hV_\alpha^{(1)} - V_\alpha^{(2)} + \sum_{k=1}^{N-1} b_{\gamma\alpha}^k\bigg\{\frac{1}{h}V_\gamma^{(1)} - Q_\gamma^k\bigg\}$$

$$R_{\alpha\beta} = R_{\alpha\beta}^{(3)} - \frac{3}{2}hR_{\alpha\beta}^{(2)} + \sum_{k=1}^{N-1} a_{\gamma\alpha}^k\bigg\{-\frac{1}{h}R_{\gamma\beta}^{(2)} + \overline{M}_{\gamma\beta}^k\bigg\}$$

$$V_\alpha = 3V_\alpha^{(2)} - 3hV_\alpha^{(1)} + \sum_{k=1}^{N-1} a_{\gamma\alpha}^k\bigg\{Q_\gamma^k + \frac{1}{h}V_\gamma^{(1)}\bigg\}$$

$$\big[F_\alpha^0 \quad F_\alpha^1\big] = \int_0^h D_\alpha\big[1 \quad z\big][H(z-z_0) - H(z-z_1)]\,\mathrm{d}z, \quad F_3^0 = \int_0^h D_3[H(z-z_0) - H(z-z_1)]\,\mathrm{d}z$$

$$\left[F_\alpha^{(N)0} \quad F_\alpha^{(N)1}\right] = \int_0^h D_\alpha\left[1 \quad z\right][H(z-z_{N-1})]\,\mathrm{d}z, \quad F_3^{(N)0} = \int_0^h D_3[H(z-z_{N-1})]\,\mathrm{d}z$$

$$\left[N_{\alpha\beta}^H \quad R_{\alpha\beta}^{H(2)} \quad R_{\alpha\beta}^{H(3)}\right] = \int_0^h (\kappa_{\alpha\beta}\theta_{,\alpha})\left[1 \quad z^2 \quad z^3\right]\mathrm{d}z, \quad \left[V_\beta^H \quad V_\beta^{H(2)} \quad V_\beta^{H(3)}\right] = \int_0^h (\kappa_{3\beta}\theta_{,3})\left[1 \quad z^2 \quad z^3\right]\mathrm{d}z$$

$$\left[\overline{M}_{\alpha\beta}^{Hk}\right] = \int_0^h (\kappa_{\alpha\beta}\theta_{,\alpha})(z-z_k)[H(z-z_k)]\,\mathrm{d}z, \quad \left[\overline{Q}_\beta^{Hk}\right] = \int_0^h (\kappa_{3\beta}\theta_{,3})(z-z_k)[H(z-z_k)]\,\mathrm{d}z$$

$$\left[V_\alpha^{H(1)} \quad V_\alpha^{H(2)} \quad Q_\alpha^{*Hk}\right] = \int_0^h (\kappa_{\alpha3}\theta_{,\alpha})\left[z \quad z^2 \quad H(z-z_k)\right]\mathrm{d}z$$

$$\left[T^H \quad T^{H(2)} \quad T^{H(3)}\right] = \int_0^h (ST_0)\left[1 \quad z^2 \quad z^3\right]\mathrm{d}z$$

$$\left[M_3^{H(1)} \quad M_3^{H(2)} \quad S_3^{Hk}\right] = \int_0^h (\kappa_{33}\theta_{,3})\left[z \quad z^2 \quad H(z-z_k)\right]\mathrm{d}z, \quad E^{Hk} = \int_0^h (ST_0)(z-z_k)H(z-z_k)\,\mathrm{d}z$$

References

Ali, J.S.M., Bhaskar, K., Varadan, T.K., 1999. A new theory for accurate thermal/mechanical flexural analysis of symmetric laminated plates. Composite Structures 45, 227–232.

Carrera, E., 2003. Historical review of zig-zag theories for multilayered plates and shells. Applied Mechanics Review 56 (3), 287–308.

Cho, M., Oh, J., 2002. Higher order zig-zag plate theory under thermo-electric–mechanical loads combined. Composites B 34 (1), 67–82.

Cho, M., Parmerter, R.R., 1992. An efficient higher-order plate theory for laminated composites. Composite Structures 20, 113–123.

Cho, M., Parmerter, R.R., 1993. Efficient higher-order composite plate theory for general lamination comfigurations. AIAA Journal 31, 1299–1306.

Crawley, E.F., 1987. Use of piezoelectric actuators as elements of intelligent structures. AIAA Journal 25 (10), 1373–1385.

Di Sciuva, M., 1987. An improved shear-deformation theory for moderately thick multilayered anisotropic shells and plates. Journal of Applied Mechanics 54, 589–596.

Dokmeci, M.C., 1980. Recent advances, vibrations of piezoelectric crystals. International Journal of Engineering Science 18, 431–448.

Franco Correia, V.M., Aguiar Gomes, M.A., Suleman, A., Mota Soares, C.M., Mota Soares, C.A., 2000. Modeling and design of adaptive composite structures. Computer Methods in Applied Mechanics and Engineering 185, 325–346.

Ha, S.K., Keilers, C., Chang, F., 1992. Finite element analysis of composite structures containing distributed piezoceramic sensors and actuators. AIAA Journal 30 (3), 772–780.

Haozhong, G., Chattopadhyay, A., Li, J., Zhou, Xu., 2000. A higher order temperature theory for coupled thermo-piezoelectric–mechanical modeling of smart composites. International Journal of Solids & Structures 37 (44), 6479–6497.

Lee, C.K., 1990. Theory of laminated piezoelectric plates for the design of distributed sensors/actuators. Part I: Governing equations and reciprocal relationships. Journal of the Acoustical Society of America 87 (3), 1144–1158.

Mindlin, R.D., 1968. Polarization gradient in elastic dielectrics. International Journal of Solids & Structures 4 (6), 637–642.

Mitchell, J.A., Reddy, J.N., 1995. A refined hybrid plate theory for composite laminates with piezoelectric laminate. International Journal of Solids & Structures 32 (16), 2345–2367.

Ray, M.C., Bhattacharya, R., Samanta, B., 1993. Exact solution for static analysis of intelligent structures. AIAA Journal 31 (9), 1684–1691.

Reddy, J.N., 1999. On laminated composite plates with intergrated sensors and actuators. Engineering Structures 21, 568–593.

Reddy, J.N., Robbins Jr., D.H., 1993. Modeling of thick composites using a layer-wise laminate theory. International Journal for Numerical Methods in Engineering 36, 655–677.

Reddy, J.N., Robbins Jr., D.H., 1994. Theories and computational models for composite laminates. Applied Mechanics Reviews 47 (6), 147–169.

Saravanos, D.A., Heyliger, P.R., Hopkins, D.A., 1997. Layerwise mechanics and finite element for the dynamic analysis of piezoelectric composite plates. International Journal of Solids & Structures 34 (3), 359–378.

Sheikh, A.H., Topdar, P., Halder, S., 2001. An appropriate FE model for through-thickness variation of displacement and potential in thin/moderately thick smart laminates. Composite Structures 51, 401–409.

Tiersten, H.F., 1970. Radiation and confinement of electromagnetic energy accompanying the oscillation of piezoelectric crystal plates. Recent Advances in Engineering 5, 63–90.

Toledano, A., Murakami, H., 1987. A composite plate theory for arbitrary laminate configurations. Journal of Applied Mechanics 54, 181–189.